Computational and Theoretical Chemistry 1140 (2018) 14–23

Contents lists available at ScienceDirect

Computational and Theoretical Chemistry

journal homepage: www.elsevier.com/locate/comptc

Quantum-chemical and kinetic study of the reactions of the $ClSO_2$ radical with H, O, Cl, S, SCl and $ClSO_2$ in the atmosphere of Venus

Adela E. Croce, Carlos J. Cobos*

Instituto de Investigaciones Fisicoquímicas Teóricas y Aplicadas (INIFTA), Departamento de Química, Facultad de Ciencias Exactas, Universidad Nacional de La Plata, CONICET, Casilla de Correo 16, Sucursal 4, La Plata (1900), Argentina

ARTICLE INFO

Keywords:
$ClSO_2$ reactions in Venus
Quantum-chemical calculations
Statistical adiabatic channel model calculations
Transition state theory calculations

ABSTRACT

Rate constants for the reactions between the $ClSO_2$ radical and H, O, Cl, S, SCl and $ClSO_2$ were studied over the 150–700 K temperature range employing the statistical adiabatic channel model/classical trajectory approach and the canonical transition state theory on potential energy surfaces based on G4//B3LYP/6-311++G(3df,3pd) calculations. For these processes the following rate constants (in cm^3 $molecule^{-1}$ s^{-1}) are predicted: $2.71 \times 10^{-11}(T/250)^{0.47}$ ($ClSO_2 + H \rightarrow HCl + SO_2$); $7.69 \times 10^{-11}(T/250)^{0.093}$ ($ClSO_2 + O \rightarrow Cl + SO_3$); $1.44 \times 10^{-11}(T/250)^{0.47}$ ($ClSO_2 + Cl \rightarrow Cl_2SO_2$); $6.73 \times 10^{-11}(T/250)^{0.18}$ ($ClSO_2 + S \rightarrow SCl + SO_2$); $9.38 \times 10^{-13}(T/250)^{0.75}$ ($ClSO_2 + SCl \rightarrow ClS(O_2)SCl$); $2.64 \times 10^{-14}(T/250)^{0.61}$ ($2\ ClSO_2 \rightarrow (O_2)ClSSCl(O_2)$). These data are in marked contrast with those normally used for the modeling of the lower and middle atmosphere of Venus. Therefore, in the absence of experimental and theoretical investigations, the above rate constants are proposed for these studies.

1. Introduction

Sulfur-containing compounds are important components of the Venus atmosphere since the planet is completely covered with clouds of H_2SO_4 droplets at altitudes of 50–70 km. Therefore, significant changes in concentrations in this region markedly affect the chemistry of the atmosphere. Reaction (1), together with the photodissociation of sulfuryl chloride $Cl_2SO_2 + h\nu \rightarrow Cl + ClSO_2$ may play a role in the coupling of chlorine and sulfur cycles.

$$Cl + SO_2 + M \rightarrow ClSO_2 + M \quad (1)$$

In fact, a number of $ClSO_2$ reactions have been considered in the modeling of the middle atmosphere of this planet (about 60–110 km) [1,2]. Moreover, the presence of Cl_2SO_2, possibly formed by recombination of $ClSO_2$ with chlorine atoms on the surface of Io, the innermost Galilean moon of the planet Jupiter, has been recently proposed [3].

The limiting low pressure rate constant determined for reaction (1) over the 266–331 K temperature range in a fast-flow system for M = Ar is k_0 = [Ar] 2.2×10^{-34} exp (1.24 kcal mol^{-1}/RT) cm^3 $molecule^{-1}$ s^{-1} [4,5]. On the other hand, the electronic structure [6], dissociation pathways [7] and the thermal stability [8] of $ClSO_2$ have been investigated by quantum-chemical methods. The $ClSO_2$ infrared spectrum has been measured in cryogenic matrices [9]. This radical has been also generated by reaction $H + Cl_2SO_2 \rightarrow HCl + ClSO_2$ [10,11].

Number densities of about 4×10^6 and 1×10^6 molecule cm^{-3} have been estimated for $ClSO_2$ near 47 km and 84 km above the Venus surface [2]. A maximum of about 2×10^9 molecule cm^{-3} is located near 68 km. The striking absence of experimental and theoretical kinetic data for the reactions between $ClSO_2$ and the species H, O, Cl, S, SCl and $ClSO_2$, included into the Zhang et al. [1] and Krasnopolsky [2,12] mechanisms to explain the vertical concentration profiles of numerous species, is surprising. In all these reactions the formation of SO_2 has been proposed to increase their scale height near 70 km altitude from about 2.5–3.5 km,

$$ClSO_2 + H \rightarrow HCl + SO_2 \quad (2)$$

$$ClSO_2 + O \rightarrow ClO + SO_2 \quad (3)$$

$$ClSO_2 + Cl \rightarrow Cl_2 + SO_2 \quad (4)$$

$$ClSO_2 + S \rightarrow SCl + SO_2 \quad (5)$$

$$ClSO_2 + SCl \rightarrow SCl_2 + SO_2 \quad (6)$$

$$2\ ClSO_2 \rightarrow Cl_2SO_2 + SO_2 \quad (7a)$$

$$2\ ClSO_2 \rightarrow Cl_2 + 2\ SO_2 \quad (7b)$$

The oxidation of SO_2 leads to the formation of SO_3 which reacts with

* Corresponding author.
E-mail address: cobos@inifta.unlp.edu.ar (C.J. Cobos).

https://doi.org/10.1016/j.comptc.2018.07.006
Received 24 May 2018; Received in revised form 11 July 2018; Accepted 11 July 2018
Available online 17 July 2018

H_2O and contributes to the formation of the clouds of *liquid* droplets of highly *concentrated* aqueous solutions of *sulfuric acid* (75–85 by weight) [2,12,13]. The combination of reaction (1) with (7b) has been considered as the source of Cl_2SO_2 in the mesosphere of Venus [14]. On the other hand, a cycle driven by $ClSO_2$ has been suggested for the oxidation of SO_2 via the $ClS(O_2)O_2$ radical [15]. Reaction (2) contributes to balance HCl consumption by solar photolysis and through reactions with O and OH [2].

To know the contribution of a chemical reaction to the atmospheric concentration profile of the participating species, the column reaction rate (CR) is often employed. For Reactions (2)-(7a) this magnitude varies from about 2×10^7 to 5×10^{12} molecule cm^{-2} s^{-1} in the mesosphere of Venus. The higher values correspond to Reactions (4) and (7a) [2]. Another magnitude related to this is the mean altitude, which is close to 70 km for processes (2)-(7a). Both magnitudes are directly proportional to the reaction rate constants values. Therefore, reliable kinetic information as a function of the altitude (i.e., as a function of the temperature and, for recombination reactions, of the total pressure) is required for their estimation. Less important contributions of Reactions (2), (4) (5) and (7a) have been reported for the chemistry of the lower region of the Venus atmosphere. In fact, lower CR values have been calculated for altitudes ranging from 5 to 24 km, where the pressures and temperatures are considerably higher than those prevailing in the middle region of the atmosphere [16].

Rate constants for Reactions (2)-(7b) based, probably, on the structure of the molecules and on the exothermicity of the reactions, have been employed for the Venus modeling [1,2,15,16]. However, several products proposed so far appear to be questionable. The mentioned importance and, to the best of our knowledge, the nonexistent kinetic information for the reactions of $ClSO_2$ with the H, O, Cl, S, SC1 and $ClSO_2$ species led us to undertake the present quantum-chemical and kinetic investigation.

2. Computational methods

The energetics of the stable structures and transitional states was computed employing the ab initio multilevel models CBS-QB3 [17,18] and G4 [19]. Potential energy features along the association reaction pathways were also calculated at the CCSD(T)/6-311 + G(3df) level of theory [20–22]. For hydrogen containing compounds, diffuse and p and d functions were included on these atoms, 6-311++G(3df,3pd). In addition to the CBS-QB3 and G4 models which rely, respectively, on B3LYP/6-311G(2d,d,p) and B3LYP/6-31G(2df,p) molecular structures and harmonic vibrational frequencies, CBS-Q//B3LYP/311++G(3df,3pd) and G4//B3LYP/311++G(3df,3pd) calculations were carried out for comparison.

Geometry optimizations without symmetry constraints were performed using analytical gradient methods. At the calculated equilibrium structures, the harmonic vibrational frequencies were then derived via analytical second derivative methods. The Synchronous Transit-Guided Quasi-Newton (STQN) methods were employed for locating transition structures, which are characterized by only one negative vibrational frequency. The connectivity between the reactants, transition states and products was verified by intrinsic reaction coordinate (IRC) calculations, which follow the minimum energy reaction pathway in mass-weighted Cartesian coordinates. All electronic structure calculations were performed using the Gaussian set of computer codes with default integration grids [23]. No improvement in the results was observed by increasing the grid to tight limits, such that Cartesian coordinates converge at least to 10^{-4} Å.

Kinetic calculations for the barrierless association reactions of $ClSO_2$ with atomic, diatomic and polyatomic species were performed employing different statistical adiabatic channel model/classical trajectory formulations (SACM/CT) [24–26]. On the other hand, for reactions that exhibit electronic barriers, the canonical formulation of the transition state theory (CTST) was used [27]. For all cases, the required molecular information was provided by the aforementioned quantum-chemical calculations.

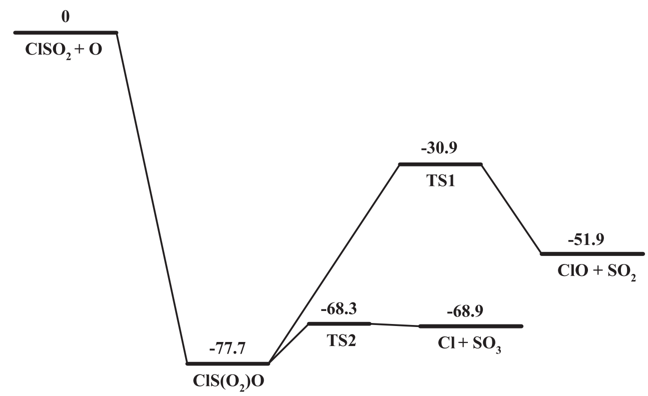

Fig. 1. Schematic diagram of the potential energy surface (in kcal mol^{-1}) calculated at the G4//B3LYP/6-311 + G(3df) level for the $ClSO_2$ + O reaction system.

3. Results and discussion

3.1. Potential energy features

To find the relevant features of the potential energy surface (PES) of each reaction of the $ClSO_2$ radical, the associative processes were first studied. As selected cases, Figs. 1 and 2 show G4//B3LYP/6-311 + G(3df) schematic potential energy diagrams corresponding to the reactions of $ClSO_2$ with O and with $ClSO_2$. It is observed that these two reactions are initiated through the formation of the $ClSO_3$ and $(O_2)ClSSCl(O_2)$ adducts bonded by 77.7 and 35.7 kcal mol^{-1}, respectively. The high content of vibrational energy of these species may be used to initiate dissociative unimolecular processes, such as those indicated for the $ClSO_2$ + O reaction, or degrade collisionally the internal energy forming the stable $(O_2)ClSSCl(O_2)$ dimer. The branching ratio between the processes that generate Cl + SO_3 and ClO + SO_2 in the first reaction, and the competition between the associative process forming the dimer and the unimolecular pathway indicated in Fig. 2 will be discussed below. Table 1 shows the energy relative to that of the input channel for all the processes calculated at different levels of theory. The computed harmonic vibrational frequencies and rotational constants for the complete series of molecular species are consigned in Table 2. It can be observed that all open-shell reaction species form excited adducts that are connected to the indicated products, through electronic barriers (transition states). By following the gradient downhill from the transition state to reactants and to products of the

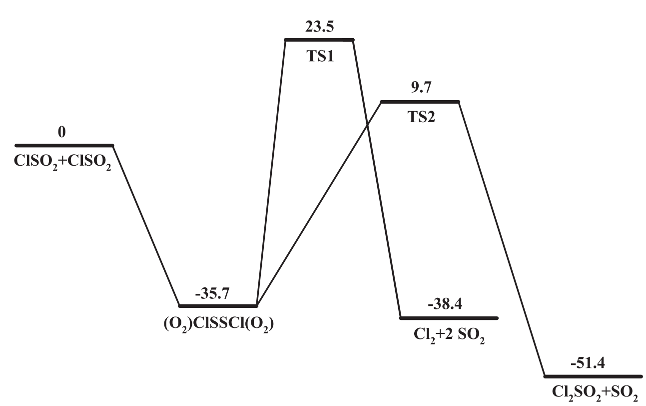

Fig. 2. Schematic diagram of the potential energy surface (in kcal mol^{-1}) calculated at the G4//B3LYP/6-311 + G(3df) level for the $ClSO_2$ + $ClSO_2$ reaction system.

Table 1
Computed reaction and transition state enthalpies at 0 K (in kcal mol^{-1}) at the CBS-QB3, CBS-Q//B3LYP/6-311 + + G(3df,3pd), G4 and G4//B3LYP/6-311 + + G(3df,3pd) levels of theory (from left to right).

Reaction	ΔH_0^0	$\Delta H_0^{\#}$
$ClSO_2$ + H → $ClS(O_2)H$	−71.3, −71.2, −71.7, −71.7	–[a]
$ClSO_2$ + H → HCl + SO_2	−92.2, −90.2, −92.6, −92.3	−36.7, −36.3, −36.4, −36.2
$ClSO_2$ + H → ClS(O)OH	−85.1, −85.2, −85.1, −85.0	7.5, 14.7, 5.6, 11.8
$ClSO_2$ + O → $ClS(O_2)O$	−77.1, −76.3, −78.4, −77.7	–[a]
$ClSO_2$ + O → ClO + SO_2	−51.4, −50.7, −52.6, −51.9	−33.8, −32.7, −31.9, −30.9
$ClSO_2$ + O → Cl + SO_3	−70.4, −69.3, −71.9, −68.9	−67.2, −66.4, −69.5, −68.3
$ClSO_2$ + Cl → Cl_2SO_2	−60.1, −60.5, −60.0, −60.2	–[a]
$ClSO_2$ + Cl → Cl_2 + SO_2	−47.9, −47.5, −47.4, −47.2	15.1, 17.1, 17.4, 18.6
$ClSO_2$ + Cl → ClSO + ClO	4.6, 5.2, 5.6, 5.4	22.0, 22.2, 22.0, 22.1
$ClSO_2$ + Cl → ClS(O)OCl	−22.2, −22.7, −21.7, −21.6	4.6, 5.2, 5.6, 5.4
$ClSO_2$ + S → $ClS(O_2)S$	−49.5, −49.6, −51.7, −49.6	–[a]
$ClSO_2$ + S → SCl + SO_2	−56.0, −55.7, −56.6, −55.7	−32.1, −32.0, −31.8, −31.9
$ClSO_2$ + S → Cl + SSO_2	−25.5, −25.2, −26.7, −25.2	−24.2, −23.2, −25.3, −23.2
$ClSO_2$ + SCl → $ClS(O_2)SCl$	−47.8, −46.8, −47.9, −48.0	–[a]
$ClSO_2$ + SCl → SCl_2 + SO_2	−50.9, −50.5, −50.9, −50.7	0.14, 0.98, 1.5, 2.1
$ClSO_2$ + SCl → $ClS(O_2)S$ + Cl	17.7, 16.9, 14.2, 14.2	–[a]
2 $ClSO_2$ → $(O_2)ClSSCl(O_2)$	−33.3, −33.5, −34.9, −35.7	–[a]
2 $ClSO_2$ → Cl_2SO_2 + SO_2	−48.9, −48.8, −50.7, −51.4	10.3, 11.0, 9.8, 9.7
2 $ClSO_2$ → Cl_2 + 2 SO_2	−36.6, −35.8, −38.2, −38.4	24.6, 24.9, 24.3, 23.5

[a] Barrierless reactions with $\Delta H_0^{\#} = \Delta H_0^0$.

dissociation reactions $(O_2)ClSSCl(O_2)$ → Cl_2SO_2 + SO_2 (TS6a) and $(O_2)ClSSCl(O_2)$ → Cl_2 + 2 SO_2 (TS6b), the IRC diagrams shown in Fig. 3 were obtained. A similar behavior was observed for the other activated process. In this way, the IRC calculations indicate that the $ClSO_2$ + X (X = H, O, Cl, S, SCl and $ClSO_2$) as reactants do not connect directly to the transition states given in Tables 1 and 2.

A recent study performed on a set of 200 total atomization energies (W4-17 database, 3σ confidence intervals of 0.2 kcal mol^{-1}) shows that the G4 model gives a root mean square deviation of 0.7 kcal mol^{-1} and the CBS-QB3 model of 2.0 kcal mol^{-1} [28]. In addition, the G4 model leads to lower mean unsigned deviations for bond-making and bond-breaking reaction barriers, if geometries better than those obtained at the original B3LYP/6-31G(2df,p) level [19] are employed [29]. Therefore, we expect that our G4//B3LYP/6-311 + + G(3df,3pd) calculations lead to the most reliable energetics. These results were used for all kinetic calculations.

An inspection of the data reported in Table 1 shows that several reactions employed in the modeling of Venus [1,2,15,16] are activated processes. In fact, electronic barriers of 18.6, 2.1, 9.7 and 23.5 kcal mol^{-1} have been calculated at the G4//B3LYP/6-311 + G(3df) level for Reactions (4), (6) (7a) and (7b), respectively. As a consequence, they surely present small reaction rate constants (see below). Therefore, the collisional stabilization to form thermalized Cl_2SO_2, $ClS(O_2)SCl$ and $(O_2)ClSSCl(O_2)$ molecules is the final fate of the initially generated energized adducts. The remaining Reactions (2), (3) and (5), exhibit electronic barriers located 36.2, 30.9 and 31.8 kcal mol^{-1} below the entrance channel energy, such that the formed $ClS(O_2)H$, $ClS(O_2)O$ and $ClS(O_2)S$ energized adducts are not

Table 2
Harmonic vibrational frequencies and rotational constants (both in cm^{-1}) calculated at the B3LYP/6-311 + + G(3df,3pd) level. Transition states: TS1a for $ClS(O_2)H$ → HCl + SO_2; TS1b for $ClS(O_2)H$ → ClS(O)OH; TS2a for $ClS(O_2)O$ → ClO + SO_2; TS2b for $ClS(O_2)O$ → Cl + SO_3; TS3a for $ClS(O_2)S$ → SCl + SO_2; TS3b for $ClS(O_2)S$ → Cl + SSO_2; TS4a for Cl_2SO_2 → Cl_2 + SO_2; TS4b for Cl_2SO_2 → ClSO + ClO; TS4c for Cl_2SO_2 → ClS(O)OCl; TS5a for $ClS(O_2)SCl$ → SCl_2 + SO_2; TS6a for $(O_2)ClSSCl(O_2)$ → Cl_2SO_2 + SO_2; TS6b for $(O_2)ClSSCl(O_2)$ → Cl_2 + 2 SO_2. The transitional frequencies employed in the SACM/CT calculations are indicated between parentheses.

Species	Harmonic vibration frequencies	Rotational constants
SCl	561	0.254
$ClSO_2$	256, 271, 446, 496, 1114, 1322	0.310, 0.125, 0.0927
$ClS(O_2)H$	293, 351, 517, 535, 1016, (1089), (1191), 1430, 2570	0.301, 0.130, 0.0969
$ClS(O_2)O$	(56), (60), 303, 303, 397, 604, 1015, 1015, 1072	0.182, 0.0957, 0.0957
Cl_2SO_2	200, (268), (348), 366, 384, 551, 566, 1198, 1435	0.144, 0.0756, 0.0622
$ClS(O_2)S$	144, (191), (308), 361, 371, 516, 564, 1156, 1366	0.120, 0.0737, 0.0627
$ClS(O_2)SCl$	59, 119, (199), (250), 311, 357, 371, 527, 534, 568, 1176, 1412	0.0797, 0.0392, 0.0341
$(O_2)ClSSCl(O_2)$	33, 101, (147), (149), (233), (236), 294, 353, 355, 357, 473, 536, 542, 613, 1175, 1198, 1416, 1431	0.0578, 0.0285, 0.0248
TS1a	1189i, 190, 236, 461, 514, 896, 1163, 1431, 1977	0.301, 0.0994, 0.0784
TS1b	1288i, 228, 282, 480, 527, 783, 1021, 1166, 3682	0.259, 0.122, 0.0834
TS2a	1066i, 27, 199, 385, 448, 508, 698, 1153, 1363	0.233, 0.0783, 0.0692
TS2b	586i, 245, 335, 380, 455, 504, 777, 1161, 1397	0.178, 0.0968, 0.0940
TS3a	78i, 29, 169, 328, 346, 453, 626, 1177, 1401	0.124, 0.0576, 0.0512
TS3b	297i, 110, 131, 275, 310, 446, 600, 1157, 1387	0.110, 0.0629, 0.0523
TS4a	580i, 78, 133, 178, 220, 298, 501, 1153, 1359	0.102, 0.0619, 0.0500
TS4b	576i, 95, 222, 276, 301, 419, 467, 876, 1234	0.118, 0.0655, 0.0476
TS4c	547i, 121, 172, 220, 263, 299, 506, 1138, 1428	0.110, 0.0615, 0.0507
TS5a	350i, 68, 85, 110, 162, 189, 237, 315, 424, 517, 1168, 1379	0.0626, 0.0400, 0.0288
TS6a	334i, 31, 69, 105, 155, 183, 197, 226, 300, 320, 345, 433, 500, 520, 1151, 1163, 1363, 1428	0.0454, 0.0295, 0.0229
TS6b	420i, 50, 51, 79, 98, 102, 142, 163, 174, 195, 282, 346, 502, 522, 1158, 1169, 1370, 1375	0.0407, 0.0265, 0.0220

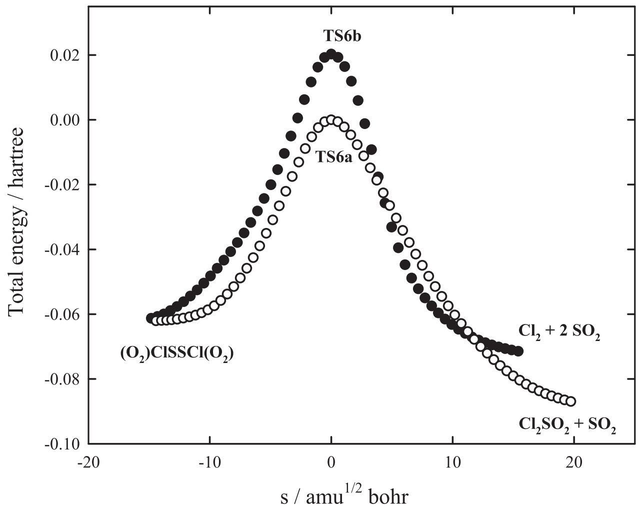

Fig. 3. IRC diagrams calculated at the B3LYP/6-311 + G(3df) level for the decomposition of the $(O_2)ClSSCl(O_2)$ excited adduct formed in the self-recombination of $ClSO_2$ radicals. See Fig. 2.

expected to be deactivated by collisions due to the fast decay into SO_2 + HCl, Cl + SO_3 and SO_2 + SCl exit channels (see below). Therefore, these reactions are dominated by the PES properties at the entrance channel, which determine the values of the high pressure rate constants, k_∞.

The potential required for the SACM/CT calculations of $k_\square$ may be divided, for convenience, in a radial or isotropic potential and an angular or anisotropic potential. The first one characterizes the reaction along the reaction coordinate while the second accounts for the transitional modes evolution along the association process. The radial potentials for the $ClS(O_2)$-H bond calculated at the G4//B3LYP/6-311 + + G(3df,3pd) and CCSD(T)/B3LYP/6-311 + + G(3df,3pd) levels are depicted in Fig. 3. As Fig. 4 shows, a similar agreement was found for the more complex $ClS(O_2)$-SCl potential. Therefore the G4//B3LYP/6-311 + + G(3df,3pd) model which provides more economic CCSD(T)/CBS energies extrapolated to the complete basis set limit (CBS) was employed for all reactions. The rest four potentials ($ClS(O_2)$-O, $ClS(O_2)$-Cl, $ClS(O_2)$-S and $(O_2)ClS$-$SCl(O_2)$) The electronic potentials for $ClS(O_2)$-O, $ClS(O_2)$-Cl, $ClS(O_2)$-S and $(O_2)ClS$-$SCl(O_2)$ are given in Figs.

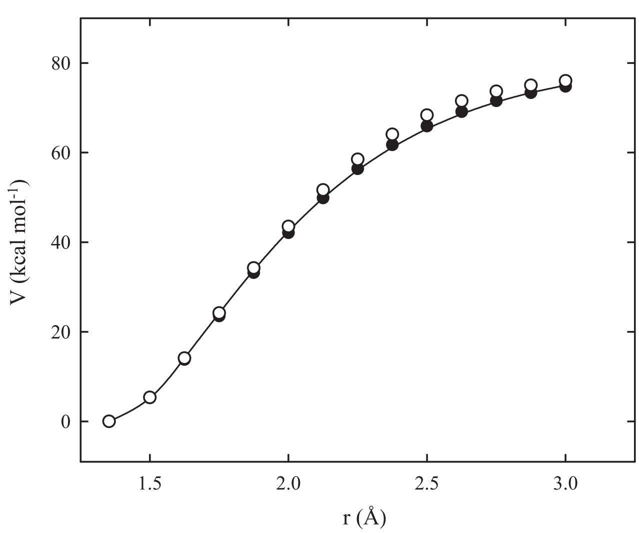

Fig. 4. Potential energy curves for $ClS(O_2)H \rightarrow ClSO_2 + H$ calculated at the G4//B3LYP/6-311 + + G(3df,3pd) (•) and CCSD(T)/B3LYP/6-311 + + G(3df,3pd) (○) levels. The solid line corresponds to a spline fit.

S1–S4 (see Supporting Information). For convenience, the angular potentials are discussed in next section.

Supplementary data associated with this article can be found, in the online version, at https://doi.org/10.1016/j.comptc.2018.07.006.

3.2. High pressure rate constants

Recombination reactions between radicals and the reverse unimolecular bond fission reactions at the high pressure limit are dominated by the intramolecular time evolution of molecules vibrationally excited above the reaction threshold. These mostly barrierless processes present a smooth transition between the reactants rotations and specific vibrational motions of the formed molecule, that is, the transitional modes. For this type of reactions, the dependence of the rate constants on the PES properties can be interpreted through the different formulations of the statistical adiabatic channel model [24–26,30–33]. In these models a Morse function for the radial potential is employed $V = D_e[1-\exp(-\beta(r-r_e)]^2$, were D_e is the bond dissociation energy, r_e the distance between the centers of mass of the two reactants and β a ranging parameter. The evolution of the transitional frequencies along the minimum energy path is described by the expression $\varepsilon(r) \approx \varepsilon(r_e)\exp[-\alpha(r-r_e)]$, where α is the so-called looseness or anisotropy parameter [30].

In particular, the more recent SACM approaches developed for atomic + linear rotor [24] and linear rotor + linear rotor [25,26] reactions enable the study of the role that the PES plays on the high pressure rate constants. These SACM/CT models, based on extensive and systematic SACM and classical trajectory (CT) calculations, allow to express the rate constants in an analytic form as a function of key PES properties. In addition, the transition from classical adiabatic (where SACM and CT match) to nonadiabatic dynamics (due to Landau-Zener-type avoided crossings) is explicitly accounted for in these formulations. It has been shown that the high pressure rate constants can be expressed as $k_\infty = f_{rigid}k_\infty^{PST}$ [33]. Here k_∞^{PST} is the phase space theory expression for k_∞ and f_{rigid} is the thermal rigidity factor. The first, which depends on the radial potential, provides an upper bound to the rate constants. $f_{rigid} \leqslant 1$, depends on both, the radial and the angular potentials and accounts for the PES anisotropy.

For nonlinear adducts formed by association of one atom and one linear rotor and for the association of two nonidentical rotors forming a nonlinear adduct, the following expression for k_∞^{PST} applies

$$k_\infty^{PST} = f_{sym}f_{el}(8\pi kT/\mu)^{1/2}[31.153018.158X+0.8685X]^2/\beta^2 \quad (8)$$

where $X = \ln(kT/D_e)-\beta r_e + 4$. μ denotes the collisional reduced mass, f_{el} the electronic degeneracy factor and f_{sym} a stoichiometric coefficient, equal to 1/2 for the association of two identical linear rotors and 1 for all other cases. On the other side, when the association of two identical rotors forms a linear adduct, the coefficients of the polynomial between brackets in Eq. (8) must be changed by −15.7706, −8.636 and 0.9975, respectively. Besides, for this case $X= \ln(kT/D_e)-\beta r_e$.

For atom + linear rotor reactions at low temperatures the reduction of the available phase space due to the PES anisotropy is accounted for by

$$f_{rigid}(T \rightarrow 0) \approx (1 + aZ^b + Z^c)^d \quad (9)$$

If a nonlinear adduct is formed by recombination of an atom and a linear rotor (as in Reactions (2)-(5)), a = 1, b = 2, c = 8, d = −1/8, $Z= (C/3\sin^2\gamma_e)^n/\gamma_1$ and $C= [1+a_1(2\alpha/\beta-1)^2 + a_2(2\alpha/\beta-1)^3](kT/D_e)^{2\alpha/\beta-1}[\varepsilon(r_e)]^2/2BD_e$ with a_1 = 0.9 and a_2 = −0.8 must be used. Here B is the rotational constant of the rotor, γ_e is the angle of the potential minimum (for the present reactions between 70 and 80°) and *n* and γ_1 are γ_e dependent parameters. Small corrections arisen from the temperature dependence of f_{rigid} are accounted for by the equation $f_{rigid}/f_{rigid}(T \rightarrow 0) = 1 - 0.94\exp(X/2.044)$ with $X = \ln(kT/D_e)-\beta r_e + 4$.

For a recombination of two identical linear rotors forming a linear complex (as in reaction 2 $ClSO_2 \rightarrow (O_2)ClSSCl(O_2)$), $f_{rigid}(T \rightarrow 0)$ is

Table 3
Morse and looseness parameters and center of mass bond distances for $ClSO_2$-X (X = H, O, Cl, S, SCl and $ClSO_2$).

Reaction	β/Å^{-1}	α/Å^{-1}	r_e/Å
$ClSO_2 + H \rightarrow ClS(O_2)H$	2.30[a]	0.72[g]	1.7
$ClSO_2 + O \rightarrow ClS(O_2)O$	2.49[b]	1.53[g]	1.9
$ClSO_2 + Cl \rightarrow Cl_2SO_2$	2.10[c]	0.71[g]	2.4
$ClSO_2 + S \rightarrow ClS(O_2)S$	2.42[d]	1.36[g]	2.4
$ClSO_2 + SCl \rightarrow ClS(O_2)SCl$	1.85[e]	0.57[g]	2.8
$2\ ClSO_2 \rightarrow (O_2)ClSSCl(O_2)$	1.94[f]	0.63[g]	3.0

[a] Fit of the potential of Fig. 3 between 2.375 and 3.125 Å.
[b] Fit of the potential of Fig. S1 between 2.25 and 2.75 Å.
[c] Fit of the potential of Fig. S2 between 2.875 and 3.625 Å.
[d] Fit of the potential of Fig. S3 between 2.75 and 3.5 Å.
[e] Fit of the potential of Fig. 4 between 3.25 and 4.0 Å.
[f] Fit of the potential of Fig. S4 between 2.25 and 4 Å.
[g] Average values obtained from Figs. S5–S10 (see Supporting Information).

given by Eq. (9), in this case with a = 1.5, b = 1, c = 4, d = −1/4. The parameters $a_1 = 0.4$ and $a_2 = 1.0$ and the symmetrical (ε_s) and asymmetrical (ε_a) deformation modes of the formed adduct must be used to calculate C, while Z= $(4C/3^{1/2})/12.5$. Corrections for the dependence of f_{rigid} with temperature can be approximated by $f_{rigid}/f_{rigid}(T \rightarrow 0) = 1 - (4C/3^{1/2})(\beta r_e)^{1/2}\exp[(X - 4)/2.044]$ with X= $\ln(kT/D_e) - \beta r_e$.

Finally, for the recombination of two nonidentical rotors forming a nonlinear complex (as in reaction $ClSO_2 + SCl \rightarrow ClS(O_2)SCl$), $f_{rigid}(T \rightarrow 0)$ is given by Eq. (9) with a = 0.75, b = 1, c = 4, d = −1/4. In the expression of C given above, $[\varepsilon(r_e)]^2/2BD_e$ must be replaced by $[[2\varepsilon_s^2\varepsilon_a^2\varepsilon_t^2/[B_1B_2(B_1 + B_1)]]^{1/3}]/2D_e$, where ε_t denotes the adduct torsional mode, and B_1 and B_2 are the fragments rotational constants. In addition Z is given by Z= C^n/γ, where γ is a function of geometry of the nonlinear adduct. For this case, $f_{rigid}/f_{rigid}(T \rightarrow 0)$ is identical to the corresponding to the association of two equal rotors forming a linear complex.

As noted, β and α are the most relevant PES parameters in the SACM formulations [24–26,30–33,34]. For the present reactions, the β values were obtained from the calculated potential energy curves (Figs. 3, 4, S1, S2, S3 and S4 (see Supporting Information)). Usually, as it is well-known, it is not possible to obtain a single β that fits the entire potential curve. For this reason, due to the fact that centrifugal and adiabatic channel barriers are located at the upper part of the potential, this relevant region was fitted to extract the effective β values listed in Table 3. On the other hand, the anisotropic potential was obtained by calculating the variation of the transitional vibrational modes as a function of the interfragment bond distances. Then, using the above given relationship (ε(r) vs. r), the corresponding α parameters were derived. The resulting decay curves are depicted in Figs. S5–S10 (see Supporting Information) while the calculated average α parameters are listed in Table 3.

It seems appropriate at this time to present the calculated k_∞ values for the association reactions of $ClSO_2$ with H, O, Cl, S, SCl and $ClSO_2$. These, and the corresponding k_∞^{PST} and f_{rigid} values are given in Table 4. The molecular input data used for these calculations are given in Tables 1 and 2. Similar to other bimolecular reactions in which energized complexes are initially formed [35–42], it is likely that the reactions of $ClSO_2$ with H, O and S atoms also pass through the formation of an intermediate complex which allows the randomization of internal energy. In these cases, the reactants, intermediary complexes and products are adiabatically connected through a ground state potential energy surface. In particular for the $ClS(O_2)O$ + O reaction (see Fig. 1 and Table 1), the first path is the formation of a vibrationally excited $ClS(O_2)O$ radical through a barrierless association reaction. At low temperatures the reverse re-dissociation reaction is normally negligible [35–37]. Therefore, once formed, this radical can be stabilized by collisions with the present gases to generate thermalized $ClS(O_2)O$,

Table 4
High pressure rate constants k_∞^{PST} and k_∞ (in cm^3 molecule^{-1} s^{-1}) and rigidity factors calculated with the SACM/CT between 150 and 300 K.

Reaction	T/K	k_∞^{PST}	f_{rigid}	k_∞
$ClSO_2 + H \rightarrow ClS(O_2)H$	150	4.18×10^{-10}	5.09×10^{-2}	2.13×10^{-11}
	200	4.58×10^{-10}	5.33×10^{-2}	2.44×10^{-11}
	250	4.91×10^{-10}	5.53×10^{-2}	2.72×10^{-11}
	300	5.20×10^{-10}	5.69×10^{-2}	2.95×10^{-11}
$ClSO_2 + O \rightarrow ClS(O_2)O$	150	7.57×10^{-11}	9.68×10^{-1}	7.33×10^{-11}
	200	7.82×10^{-11}	9.64×10^{-1}	7.54×10^{-11}
	250	8.00×10^{-11}	9.61×10^{-1}	7.69×10^{-11}
	300	8.17×10^{-11}	9.58×10^{-1}	7.82×10^{-11}
$ClSO_2 + Cl \rightarrow Cl_2SO_2$	150	5.66×10^{-11}	1.97×10^{-1}	1.12×10^{-11}
	200	6.23×10^{-11}	2.05×10^{-1}	1.28×10^{-11}
	250	6.70×10^{-11}	2.12×10^{-1}	1.42×10^{-11}
	300	7.08×10^{-11}	2.18×10^{-1}	1.54×10^{-11}
$ClSO_2 + S \rightarrow ClS(O_2)S$	150	7.68×10^{-11}	7.97×10^{-1}	6.12×10^{-11}
	200	8.29×10^{-11}	7.87×10^{-1}	6.52×10^{-11}
	250	8.69×10^{-11}	7.78×10^{-1}	6.76×10^{-11}
	300	8.97×10^{-11}	7.71×10^{-1}	6.91×10^{-11}
$ClSO_2 + SCl \rightarrow ClS(O_2)SCl$	150	4.65×10^{-10}	1.37×10^{-3}	6.38×10^{-13}
	200	5.12×10^{-10}	1.56×10^{-3}	7.97×10^{-13}
	250	5.51×10^{-10}	1.71×10^{-3}	9.41×10^{-13}
	300	5.85×10^{-10}	1.84×10^{-3}	1.07×10^{-12}
$2\ ClSO_2 \rightarrow (O_2)ClSSCl(O_2)$	150	5.01×10^{-11}	3.68×10^{-4}	1.84×10^{-14}
	200	5.53×10^{-11}	4.13×10^{-4}	2.28×10^{-14}
	250	5.96×10^{-11}	4.44×10^{-4}	2.64×10^{-14}
	300	6.33×10^{-11}	4.64×10^{-4}	2.94×10^{-14}

or to overcome barriers to form the products Cl + SO_3 or ClO + SO_2. The competence between the collisional deactivation rate $k_d[M]$ and the energy-dependent specific rate constant k(E) determines the fate of the excited $ClS(O_2)O$. k_d may be estimated as $k_d \approx \beta_c Z_{LJ}$, where Z_{LJ} is the Lennard-Jones collision frequency between $ClS(O_2)O$ and the Venus bath gas M = CO_2, and β_c the collision efficiency for this process. For a mean altitude of about 70 km (230 K and 1×10^{18} molecule cm^{-3}), typical values of $Z_{LJ} \approx 4 \times 10^{-10}$ cm^3 molecule^{-1} s^{-1} and $\beta_c \approx 0.5$, lead to a collisional rate of $k_d[CO_2] \approx 2\times10^8$ s^{-1}.

For the estimation of the thermalized specific rate constants, the Forsť inverse Laplace transform approach was employed: $k(E) = A_\infty \rho(E - E_\infty)/\rho(E)$ [43]. At the high threshold energies of the present adducts, the Whitten-Rabinovitch approximation for the $\rho(E - E_\infty)$ and for the ρ vibrational density of states applies very well [44]. In this way, the expression $k(E) = A_\infty[(E - E_\infty + a(E - E_\infty)E_Z)/(E + a(E)E_Z)]^{s-1}$ is obtained. Here A_∞ and E_∞ denote the Arrhenius preexponential factor and the activation energy for the dissociating adduct at the high pressure limit, E is their total energy, $a(E - E_\infty)E_Z$ and $a(E)$ are correction factors to the zero-point vibrational energy E_Z, and s = 9 the number of oscillators. The high pressure rate constants for the adduct decompositions $ClS(O_2)H \rightarrow HCl + SO_2$, $ClS(O_2)O \rightarrow ClO + SO_2$, $ClS(O_2)O \rightarrow Cl + SO_3$, $ClS(O_2)S \rightarrow SCl + SO_2$ and $ClS(O_2)S \rightarrow Cl + SSO_2$ together with their respective Arrhenius parameters are summarized in Table S1 of the Supporting Information. The derived $k(E)$ values as a function of the redistributable energy $E - E_\infty$ are listed in Table 5. These results

Table 5
Specific rate constants (in s^{-1}) for the dissociation of the energized adducts as a function of the redistributable energy (in kcal mol^{-1}). See text.

Reaction	$E - E_\infty$	k(E)
$ClS(O_2)H \rightarrow HCl + SO_2$	32.1	1.6×10^{11}
$ClS(O_2)O \rightarrow ClO + SO_2$	30.7	2.3×10^{10}
$ClS(O_2)O \rightarrow Cl + SO_3$	68.4	4.4×10^{11}
$ClS(O_2)S \rightarrow SCl + SO_2$	31.9	2.8×10^{12}
$ClS(O_2)S \rightarrow Cl + SSO_2$	23.2	1.5×10^{11}

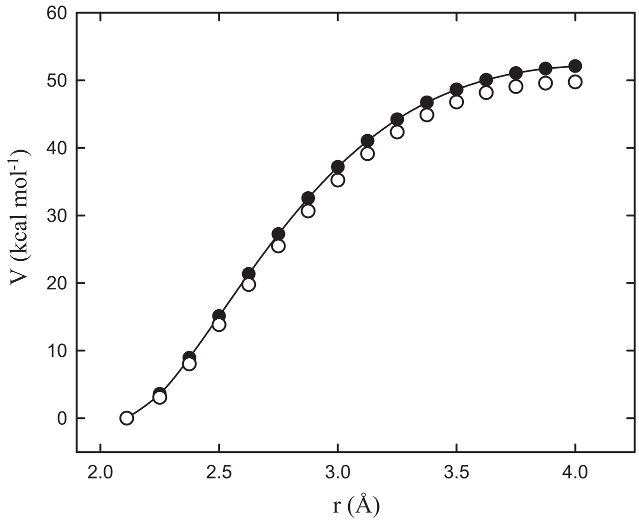

Fig. 5. Potential energy curves for $ClS(O_2)SCl \rightarrow ClSO_2 + SCl$ calculated at the G4//B3LYP/6-311 + G(3df) (•) and CCSD(T)/B3LYP/6–311 + G(3df) (○) levels. The solid line corresponds to a spline fit.

indicate that, under the Venus atmospheric conditions, the microcanonical rate constants $k(E)$ are about 1×10^2 to 1×10^4 times larger than the above estimated collisional stabilization rate of $k_d[CO_2] \approx 2\text{x}10^8\ s^{-1}$ and, in consequence, the above dissociative processes are clearly dominant. In addition, it can be observed that the $ClS(O_2)O \rightarrow Cl + SO_3$ reaction exhibits a $k(E)$ value near 20 times larger than the corresponding to $ClS(O_2)O \rightarrow ClO + SO_2$ reaction. Hence, the initial radical recombination to form the $ClS(O_2)O$ adduct is the rate-controlling process and the overall rate constant approaches the capture rate constant (the high pressure rate constant) for the $ClSO_2 + O \rightarrow Cl + SO_3$ pathway. As it can be inferred from the enthalpy values listed in Table 1, the reactions between the $ClSO_2$ radical and the H and S atoms show a similar behavior. The calculated rate constants for the reactions $ClSO_2 + H \rightarrow HCl + SO_2$, $ClSO_2 + O \rightarrow Cl + SO_3$, and $ClSO_2 + S \rightarrow SCl + SO_2$ are listed in Table 4. The optimized structures of the formed intermediate adducts $ClS(O_2)H$, $ClS(O_2)O$ and $ClS(O_2)S$ are depicted in Fig. 5.

3.3. Pressure dependence of the rate constants

The presence of the electronic barriers in the Reactions (4), (6), (7a) and (7b) and in the reactions $ClSO_2 + X$ (X = Cl, SCl and $ClSO_2$) given in Fig. 2 and in Table 1 indicates that the Cl_2SO_2, $ClS(O_2)SCl$ and $(O_2)ClSSCl(O_2)$ energized adducts formed in the reactions of $ClSO_2$ with Cl, SCl and $ClSO_2$ must be collisionally stabilized (See Fig. 6). Therefore, the pressure dependence of the corresponding recombination rate constants must be investigated. For this, the Troe's factorized formalism was employed [45]. At the low pressure limit, the recombination rate constant can be expressed as $k_0 = \beta_c k_0^{SC}$, wherek_0^{SC} is the so-called strong-collision rate constant,

$$k_0 = \beta_c(1/K_C)[\mathrm{M}]Z_{LJ}\frac{\rho_{vib,h}(E_0)kT}{Q_{vib}}exp\left(-\frac{E_0}{kT}\right)F_{anh}F_E F_{rot}F_{rotint} \quad (10)$$

Here, $K_C = [ClSO_2][X]/[ClSO_2X]$ (X = Cl, SCl and $ClSO_2$) is the equilibrium constant, $E_0 \approx \Delta_0 H^0$ is the threshold energy, $\rho_{vib,h}(E_0)$ is the harmonic vibrational density of states of $ClSO_2X$ and Q_{vib} is the corresponding vibrational partition function. The factor F_{anh} accounts for the anharmonicity, F_E takes into consideration the energy dependence of $\rho_{vib,h}(E_0)$, F_{rot} describes the contribution of the external rotations, and F_{rotint} takes into account the internal rotors behavior. For simplicity, the analytical expressions of each of these factors, given in Ref. [45], were not included in this work. Their evaluation was performed using the molecular data listed in Tables 1 and 2. The

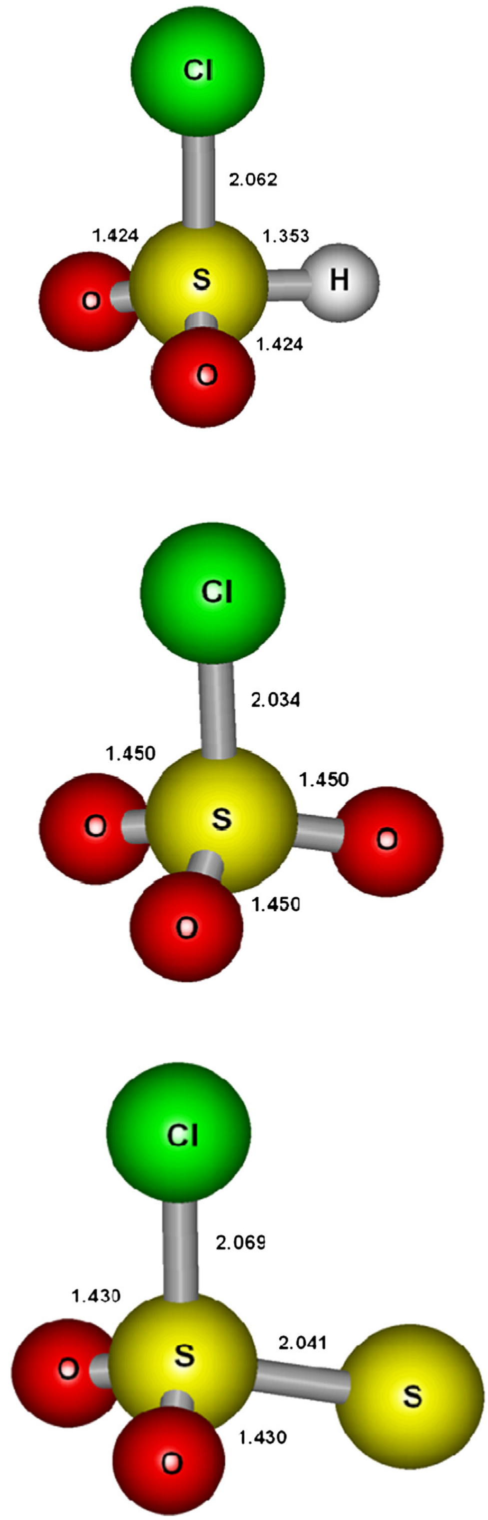

Fig. 6. Molecular structures for the $ClS(O_2)H$, $ClS(O_2)O$ and $ClS(O_2)S$) adducts optimized at the B3LYP/6-311 + +G(3df,3df) level. Bond distances in angstroms, angles in degrees.

calculations were carried out for M = CO_2. The β_c values were obtained from the relationship $-\langle\Delta E\rangle \approx F_E kT\beta_c/(1-\beta_c^{1/2})$ [46], using a temperature independent average energy transferred in up and down $ClSO_2X$-CO_2 collisions of $-\langle\Delta E\rangle = 300\ cm^{-1}$, which was based on direct energy transfer experiments [47–51]. This value compares very well with the recently derived for reaction $ClCO + O_2 + CO_2 \rightarrow ClC(O)OO + CO_2$ of $275\ cm^{-1}$ [42]. The individual factors of Eq. (10) and the

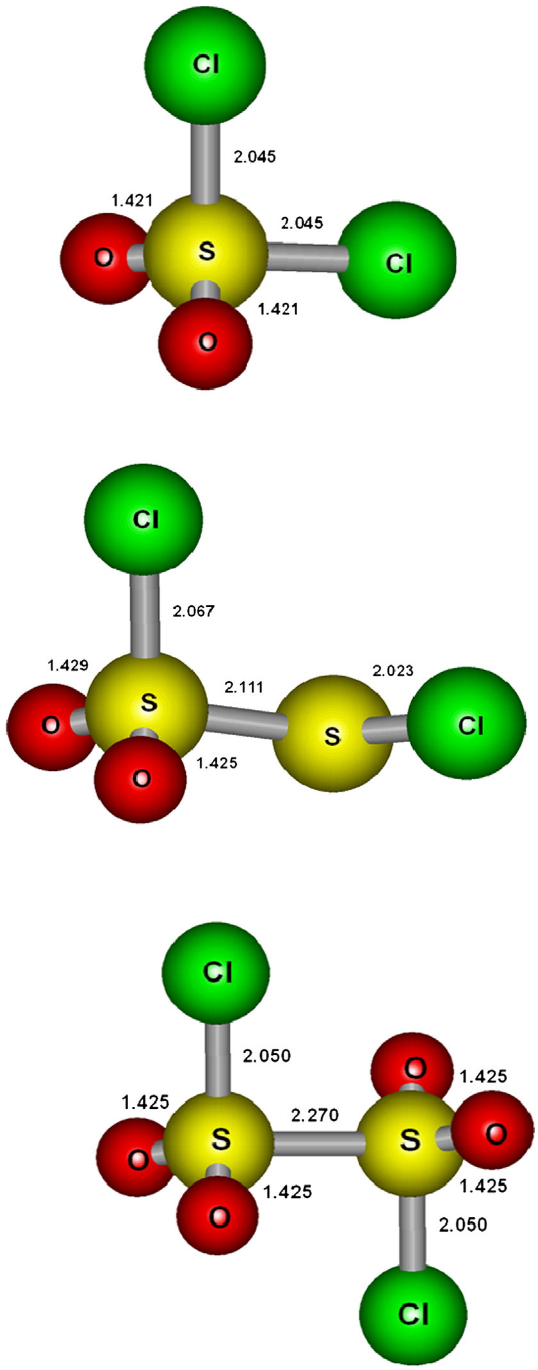

Fig. 7. Molecular structures for the Cl_2SO_2, $ClS(O_2)SCl$ and $(O_2)ClSSCl(O_2)$ molecules optimized at the B3LYP/6-311 + G(3df) level. Bond distances in angstroms, angles in degrees.

resulting k_0 values are summarized in Tables S2, S3 and S4 (see Supporting Information). Between 150 and 300 K the k_0 expressions obtained for the reactions $ClSO_2 + Cl + CO_2 \rightarrow Cl_2SO_2 + CO_2$, $ClSO_2 + SCl + CO_2 \rightarrow ClS(O_2)SCl + CO_2$ and $2\ ClSO_2 + CO_2 \rightarrow (O_2)ClSSCl(O_2) + CO_2$ are $[CO_2]1.40 \times 10^{-27}(T/250)^{-2.86}$, $[CO_2]9.34 \times 10^{-28}(T/250)^{-6.03}$ and $[CO_2]3.27 \times 10^{-28}(T/250)^{-6.35}$ cm^3 $molecule^{-1}$ s^{-1}, respectively.

At this stage we may explore the pressure dependence of the rate constants of the above recombination reactions. In the intermediate falloff range, a smooth transition between the low- and the high-pressure rate constants is observed. To model this, the Troés reduced method for falloff curves was employed [52]. The main expression for

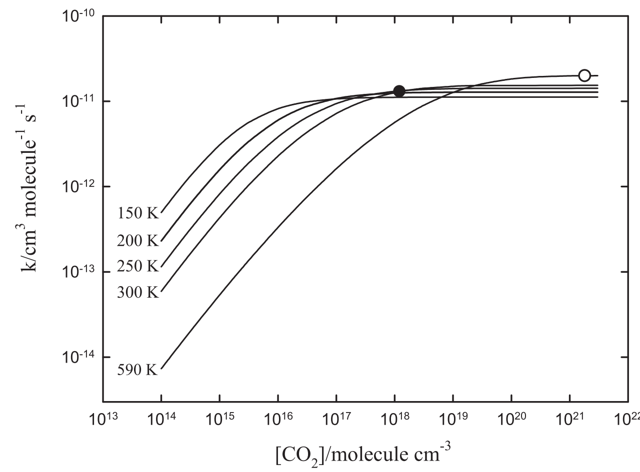

Fig. 8. Falloff curves for the reaction $ClSO_2 + Cl + CO_2 \rightarrow Cl_2SO_2 + CO_2$. (•): Rate constant calculated at the middle atmosphere Venus conditions: T ≈ 230 K and $[CO_2] \approx 1 \times 10^{18}$ molecule cm^{-3}. (○): Rate constant calculated at the lower atmosphere Venus conditions: T ≈ 590 K and $[CO_2] \approx 1.8 \times 10^{21}$ molecule cm^{-3}.

the rate constants is

$$k = k_\infty x/(1 + x)F(x) \tag{11}$$

where $x = k_0/k_\infty$ and $F(x) = (1 + x)/(1 + x^n)^{1/n}$. In this last equation $n = [\ln 2/\ln(2/F_{cent})](0.8 + 0.2x^q)$, being $q = (F_{cent}-1)/\ln(F_{cent}/10)$ and $F_{cent} = F(x = 1) = F_{cent}^{SC}F_{cent}^{WC}$. The strong collision factor $F_{cent}{}^{SC}$ was calculated using the vibrational frequencies for the adducts listed in Table 2 [53], while the weak collision factor is given by $F_{cent}^{WC} = \beta_c^{0.14}$ [54].

The resulting falloff curves obtained employing the k_∞ and k_0 values listed in Tables 4, S2, S3 and S4 (see Supporting Information) are shown in Figs. 7–9. As it can be observed, at about 70 km, where the $ClSO_2$ radical exhibits its maximum concentration (T ≈ 230 K and ($[CO_2] \approx 1 \times 10^{18}$ molecule cm^{-3}) the $ClSO_2 + Cl + CO_2 \rightarrow Cl_2SO_2 + CO_2$ reaction presents a rate constant of 1.3×10^{-11} cm^3 $molecule^{-1}$ s^{-1}, which is comparable with the SACM/CT predicted value of 1.4×10^{-11} cm^3 $molecule^{-1}$ s^{-1} (k_0 = $[CO_2]$ 1.8×10^{-27} cm^3 $molecule^{-1}$ s^{-1}).

Falloff effects are not expected neither for reaction $ClSO_2 + SCl + CO_2 \rightarrow ClS(O_2)SCl + CO_2$ nor for $2\ ClSO_2 + CO_2 \rightarrow (O_2)ClSSCl(O_2) + CO_2$. The calculated rate constants of 8.7×10^{-13} and 2.5×10^{-14} cm^3 $molecule^{-1}$ s^{-1} are identical to those predicted by the SACM/CT at 230 K. Therefore, the three recombination reactions

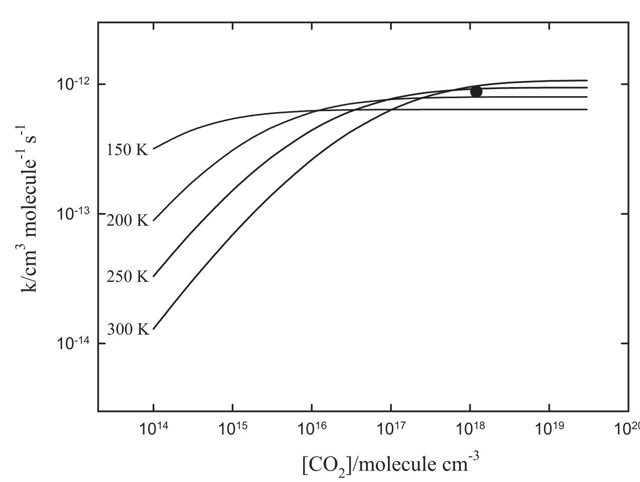

Fig. 9. Falloff curves for the reaction $ClSO_2 + SCl + CO_2 \rightarrow ClS(O_2)SCl + CO_2$. (•): Rate constant calculated at the middle atmosphere Venus conditions: T ≈ 230 K and $[CO_2] \approx 1 \times 10^{18}$ molecule cm^{-3}.

Table 6
Calculated rate constants (in cm^3 $molecule^{-1}$ s^{-1}) for the $ClSO_2$ + X (X = H, O, Cl, S, SCl and $ClSO_2$) reactions at 230 K. [a] Estimated in Ref. [1]. [b] Estimated in Ref. [2]. [c] Estimated in Ref.[12]. [d] Estimated in Ref. [15]. [e] SACM/CT calculations from this work. [f] CTST calculations from this work.

Reaction	Rate constant	Rate constant	Reaction	Rate constant
$ClSO_2 + H \rightarrow HCl + SO_2$	$1 \times 10^{-11a,b,c}$	2.6×10^{-11e}	$ClSO_2 + H \rightarrow HCl + SO_2$	2.6×10^{-11e}
$ClSO_2 + O \rightarrow ClO + SO_2$	1×10^{-12b} 1×10^{-11a}	7.6×10^{-11e}	$ClSO_2 + O \rightarrow Cl + SO_3$	7.6×10^{-11e}
$ClSO_2 + Cl \rightarrow Cl_2 + SO_2$	$1 \times 10^{-12b,c}$ 1×10^{-20a}	4.4×10^{-31f}	$ClSO_2 + Cl \rightarrow Cl_2SO_2$	1.4×10^{-11e}
$ClSO_2 + S \rightarrow SCl + SO_2$	1×10^{-11a}	6.7×10^{-11e}	$ClSO_2 + S \rightarrow SCl + SO_2$	6.7×10^{-11e}
$ClSO_2 + SCl \rightarrow SCl_2 + SO_2$	1×10^{-13b} $5 \times 10^{-12a,d}$	3.0×10^{-17f}	$ClSO_2 + SCl \rightarrow ClS(O_2)SCl$	8.7×10^{-13e}
$2\ ClSO_2 \rightarrow Cl_2SO_2 + SO_2$	$1 \times 10^{-12b,c}$	5.9×10^{-26f}	$2\ ClSO_2 \rightarrow (O_2)ClSSCl(O_2)$	2.5×10^{-14e}
$2\ ClSO_2 \rightarrow Cl_2 + 2\ SO_2$	5×10^{-13a}	2.7×10^{-38f}	–	–

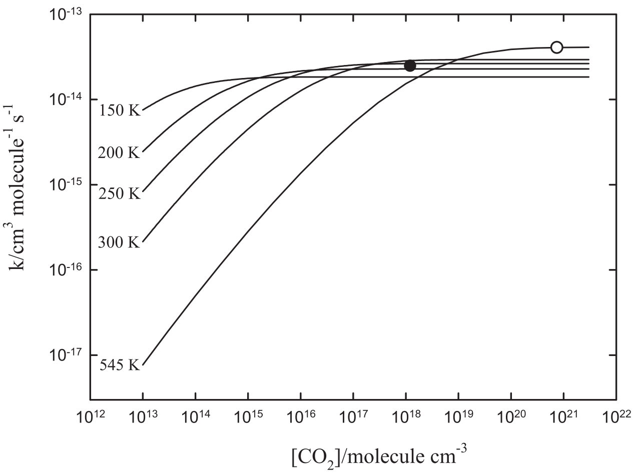

Fig. 10. Falloff curves for the reaction 2 $ClSO_2$ + CO_2 → $(O_2)ClSSCl(O_2)$ + CO_2. (•): Rate constant calculated at the middle atmosphere Venus conditions: T ≈ 230 K and $[CO_2]$ ≈ 1×10^{18} molecule cm^{-3}. (○): Rate constant calculated at the lower atmosphere Venus conditions: T ≈ 545 K and $[CO_2]$ ≈ 7.4×10^{20} molecule cm^{-3}.

are very close to their respective high pressure limits and no appreciable falloff effects are expected at the middle atmosphere of Venus.

3.4. Atmospheric implications

The rate constants for the $ClSO_2$ Reactions (2)-(7b) proposed by Zhang et al. [1] (modeling with 341 reactions) and Krasnopolsky [2,12] (modeling with 153 reactions) to model the middle atmosphere of Venus were compared with those resulting from the present theoretical study. The CTST rate constants obtained over the 150–300 K range are listed in Table S5 (see Supporting Information), while values derived from CTST and SACM/CT calculations at 230 K are reported in Table 6. As it can be seen, large discrepancies, of up to several orders of magnitude, between the rate constants proposed in Refs. [1,2,12], and our values were found. These differences could be attributed to the presence of important electronic barriers (see Table 1), certainly not taken into account in the kinetic estimates of Zhang et al. [1] and Krasnopolsky [2,12].

Reactions (2), (4), (5) and (7) have also been included in the modeling of the lower venusian atmosphere [16]. The estimated average heights where these processes predominate are 5, 14, 23 and 24 km, respectively. At these altitudes the prevailing temperatures are close to 700, 590, 550 and 545 K, respectively. As it can be observed in Table 6, the rate constant values employed in Ref. [16] for Reactions (2), (4) and (7) are identical to those used at 230 K. On the other hand, a value of 1×10^{-11} cm^3 $molecule^{-1}$ s^{-1} was used for reaction $ClSO_2 + S \rightarrow SCl + SO_2$, which is an order of magnitude higher than that estimated by Zhang et al. [1]. As Figs. 8 and 10 show, no pressure dependence of the rate constants for the reaction of $ClSO_2$ with Cl and $ClSO_2$ are predicted at the high pressures and temperatures predominant at the lower atmosphere. Consequently, the rate constants for these four processes were calculated with the SACM/CT and CTST approaches as before. The obtained values are listed in Table 7.

At this time the role that the rate constants play on the column reaction rates should be emphasized. This magnitude is defined as $CR = \int k(h)(1 + h/R_0)^2 dh$, where $k(h)$ is the rate constant as a function of the altitude h (that is, as a function of temperature and total pressure) [2]. The surface radius of Venus is R_0 = 6052 km and the integration limits extend from 47.5 to 111.5 km, for the middle atmosphere, and from 1 to 46 km for the lower atmosphere. Our kinetic results indicate that the CR values calculated for Reactions (2), (3), (4), (6) and (7a) in the middle atmosphere of 3.55×10^9, 5.56×10^{11}, 5.14×10^{12}, 2.32×10^7 and 2.31×10^{12} molecule cm^{-2} s^{-1} [10] should be corrected according to the rate constants listed in columns 2 and 5 of Table 6. In addition, the CR values derived in Ref. [16] for the lower atmosphere of 3.03×10^7 (Reaction (2) at 5 km), 7.19×10^8 (Reaction (4) at 14 km), 2.64×10^9 (Reaction (5) at 23 km) and 3.44×10^9–1.36×10^{14} molecule cm^{-2} s^{-1} (Reaction (7) at 24 km) should also be scaled by the rate constants values listed in Table 7. Besides, the reaction products of Reactions (3), (4), (6) and (7) should be accordingly modified. According to our kinetic results (Table 6), the CR values calculated by Krasnopolsky for Reactions (2), (3), (4), (6) and (7a) in the middle atmosphere of 3.55×10^9, 5.56×10^{11}, 5.14×10^{12}, 2.32×10^7 and 2.31×10^{12} molecule cm^{-2} s^{-1} [2] should be changed to 9.2×10^9, 4.2×10^{13}, 7.2×10^{13}, 2.0×10^8 and 5.8×10^{10} molecule cm^{-2} s^{-1}. In addition, the CR values derived in Ref. [16] for the lower atmosphere of 3.03×10^7 (Reaction (2) at 5 km), 7.19×10^8 (Reaction (4) at 14 km), 2.64×10^9 (Reaction (5) at 23 km) and 3.44×10^9–1.36×10^{14} molecule cm^{-2} s^{-1} (Reaction (7) at 24 km),

Table 7
Calculated rate constants (in cm^3 $molecule^{-1}$ s^{-1}) for the $ClSO_2$ + X (X = H, Cl, S, and $ClSO_2$) reactions. [a]Estimated in Ref. [16]. [b]SACM/CT calculations from this work. [c]CTST calculations from this work. [d]At 700 K. [e]At 590 K. [f]At 550 K. [g]At 545 K. Calculated rate constants (in cm^3 $molecule^{-1}$ s^{-1}) for the $ClSO_2$ + X (X = H, O, Cl, S, SCl and $ClSO_2$) reactions at 230 K.

Reaction	Rate constant	Rate constant	Reaction	Rate constant
$ClSO_2 + H \rightarrow HCl + SO_2$	1×10^{-11a}	$4.3 \times 10^{-11b,d}$	$ClSO_2 + H \rightarrow HCl + SO_2$	$4.3 \times 10^{-11b,d}$
$ClSO_2 + Cl \rightarrow Cl_2 + SO_2$	1×10^{-12a}	$6.0 \times 10^{-20c,e}$	$ClSO_2 + Cl \rightarrow Cl_2SO_2$	$2.0 \times 10^{-11b,e}$
$ClSO_2 + S \rightarrow SCl + SO_2$	1×10^{-12a}	$7.2 \times 10^{-11b,f}$	$ClSO_2 + S \rightarrow SCl + SO_2$	$7.2 \times 10^{-11b,f}$
$2\ ClSO_2 \rightarrow Cl_2SO_2 + SO_2$	1×10^{-12a}	$2.9 \times 10^{-20c,g}$	$2\ ClSO_2 \rightarrow (O_2)ClSSCl(O_2)$	$4.1 \times 10^{-14b,g}$

once scaled by the rate constants listed in Table 7 should be, respectively, 1.3×10^{8}, 1.4×10^{10}, 1.9×10^{11} and 2.5×10^{11}–9.8×10^{15} molecule $cm^{-2}\ s^{-1}$. Moreover, the reaction products of Reactions (3), (4), (6) and (7) have to be modified accordingly. It should be noted that only 7 of the 153 thermal reactions included in the Krasnopolsky's mechanism of the middle atmosphere of Venus present CR values larger than 10^{13} molecule $cm^{-2}\ s^{-1}$ [2]. On the other hand, 15 of the 89 reactions that have been proposed for the low atmosphere mechanism exhibit CR larger than this last value [16].

Finally, we would like to discuss briefly the relative relevance of the two proposed cycles for the $ClSO_2$ radical [15]. The first one is constituted by the reactions $Cl + SO_2 + CO_2 \rightarrow ClSO_2 + CO_2$, $ClSO_2 + O_2 + CO_2 \rightarrow ClS(O_2)OO + CO_2$, $ClS(O_2)OO + Cl \rightarrow SO_3 + ClO + Cl$ and $SO_3 + H_2O + CO_2 \rightarrow H_2SO_4 + CO_2$. This cycle might be important if the rate constant for the reaction forming $ClS(O_2)OO$ were greater than $[CO_2]$ 3×10^{-32} cm^3 $molecule^{-1}$ s^{-1} [15]. Unfortunately, no kinetic data has been reported for this process. On the other hand, according to the present results, the participation of the second postulated cycle: $2(Cl + SO_2 + CO_2 \rightarrow ClSO_2 + CO_2)$ and $2\ ClSO_2 \rightarrow Cl_2SO_2 + SO_2$ [15], should be discarded. In fact, as Table 6 shows, a value of 5.9×10^{-26} cm^3 $molecule^{-1}$ s^{-1} has been calculated for this last reaction at 230 K, while $2\ ClSO_2 \rightarrow (O_2)ClSSCl(O_2)$ results the predominant reaction channel with a high pressure rate constant of 2.5×10^{-14} cm^3 $molecule^{-1}$ s^{-1}.

4. Conclusions

The present quantum-chemical and kinetic study allows to predict rate constants for a series of reactions between the $ClSO_2$ radical and species of importance in the lower and middle atmosphere of Venus. On the basis of relevant potential energy surface features computed at the G4//B3LYP/6-311++G(3df,3pd) level, SACM/CT kinetic calculations for the reactions of $ClSO_2$ with H, O, Cl, S, SCl and $ClSO_2$ were performed. The predicted reactions and their associated rate constants (in cm^3 $molecule^{-1}$ s^{-1}) over the 150–300 K range are

$$ClSO_2 + H \rightarrow HCl + SO_2 \quad k = 2.71 \times 10^{-11}\ (T/250)_{0.47}$$

$$ClSO_2 + O \rightarrow Cl + SO_3 \quad k = 7.69 \times 10^{-11}(T/250)^{0.093}$$

$$ClSO_2 + Cl \rightarrow Cl_2SO_2 \quad k = 1.44 \times 10^{-11}(T/250)^{0.47}$$

$$ClSO_2 + S \rightarrow SCl + SO_2 \quad k = 6.73 \times 10^{-11}(T/250)^{0.18}$$

$$ClSO_2 + SCl \rightarrow ClS(O_2)SCl \quad k = 9.38 \times 10^{-13}(T/250)^{0.75}$$

$$ClSO_2 \rightarrow (O_2)ClSSCl(O_2) \quad k = 2.64 \times 10^{-14}\ (T/250)^{0.61}$$

At higher temperatures, as those prevailing in the lower venusian atmosphere, the rate constants for the reactions of $ClSO_2$ with H, Cl, S and $ClSO_2$ (see Table 7) are also very well reproduced by the above expressions. These kinetic data, which are based on reliable and validated theoretical models, largely disagree with those employed in current modeling studies of Venus [1,2,12,16]. Therefore, in the absence of experimental information we propose their use for atmospheric studies.

Acknowledgements

This research project was supported by the Universidad Nacional de La Plata (11/X676), the Consejo Nacional de Investigaciones Científicas y Técnicas CONICET (PIP 2012-0134) and the Agencia Nacional de Promoción Científica y Tecnológica (PICT 2012-0478).

References

[1] X. Zhang, M.C. Liang, F.P. Mills, D.A. Belyaev, Y.L. Yung, Sulfur chemistry in the middle atmosphere of Venus, Icarus 217 (2012) 714–739.
[2] V.A. Krasnopolsky, A photochemical model for the Venus atmosphere at 47–112 km, Icarus 218 (2012) 230–246.
[3] B. Schmitt, S. Rodriguez, Possible identification of local deposits of Cl_2SO_2 on Io from NIMS/Galileo spectra, J. Geophys. Res. 108 (2003) 5104.
[4] L.W. Strattan, R.E. Eibling, M. Kaufman, Rate constant of the reaction between chlorine atoms and sulfur dioxide and its significance for stratospheric chlorine chemistry, Atmos. Environ. 13 (1979) 175–177.
[5] R.E. Eibling, M. Kaufman, Kinetics studies relevant to possible coupling between the stratospheric chlorine and sulfur cycles, Atmos. Environ. 17 (1983) 429–431.
[6] Z. Li, Ab Initio study of the electronic structure of XSO and XSO_2 (X = F, Cl) radicals, J. Phys. Chem. A. 101 (1997) 9545–9550.
[7] Z. Li, Ab initio study on the dissociation pathways of XSO_2 (X = Cl, F) radicals, Chem. Phys. Lett. 269 (1997) 128–137.
[8] A.F. Khalizov, P.A. Ariya, Stability of XSO_2 (X = F, Cl, and Br) radical: impact of the basis set on X-S bonding energy in ab initio and DFT calculations, Chem. Phys. Lett. 350 (2001) 173–180.
[9] M. Bahou, S.-F. Chen, Y.-P. Lee, Production and infrared absorption spectrum of $ClSO_2$ in matrices, J. Phys. Chem. A 104 (2000) 3613–3619.
[10] M.J. Perona, D.W. Setser, R.J. Johnson, Infrared chemiluminescence from the reaction of hydrogen atoms with SCl_2, S_2Cl_2, $SOCl_2$, SO_2Cl_2, and OCl_2, J. Chem. Phys. 52 (1970) 6384–6390.
[11] J.P. Sung, D.W. Setser, Comparisons of the energy disposal by the reactions of H atoms with Cl_2, SCl_2, S_2Cl_2, and SO_2Cl_2 from observation of the HCl infrared chemiluminescence, Chem. Phys. Lett. 58 (1978) 98–103.
[12] V.A. Krasnopolsky, Chemical kinetic model for the lower atmosphere of Venus, Icarus 191 (2007) 25–37.
[13] X. Zhang, M.C. Liang, F. Montmessin, J.L. Bertaux, C. Parkinson, Y.L. Yung, Photolysis of sulphuric acid as the source of sulphur oxides in the mesosphere of Venus, Nat. Geosci. 3 (2010) 834–837.
[14] W.B. DeMore, M.T. Leu, R.H. Smith, Y.L. Yung, Laboratory studies on the reactions between chlorine, sulfur dioxide, and oxygen: implications for the Venus Stratosphere, Icarus 63 (1985) 347–353.
[15] F.P. Mills, M. Allen, A review of selected issues concerning the chemistry in Venus middle atmosphere, Planet. Space Sci. 55 (2007) 1729–1740.
[16] V.A. Krasnopolsky, S3 and S4 abundances and improved chemical kinetic model for the lower atmosphere of Venus, Icarus 225 (2013) 570–580.
[17] J.A. Montgomery Jr., M.J. Frisch, J.W. Ochterski, G.A. Petersson, A complete basis set model chemistry. VI. Use of density functional geometries and frequencies, J. Chem. Phys. 110 (1999) 2822–2827.
[18] J.A. Montgomery Jr., M.J. Frisch, J.W. Ochterski, G.A. Petersson, A complete basis set model chemistry. VII. Use of the minimum population localization method, J. Chem. Phys. 112 (2000) 6532–6542.
[19] L.A. Curtiss, P.C. Redfern, K. Raghavachari, Gaussian-4 theory, J. Chem. Phys. 126 (2007) 084108.
[20] M. Urban, J. Noga, S.J. Cole, R.J. Bartlett, Towards a full CCSDT model for electron correlation, J. Chem. Phys. 83 (1985) 4041–4046.
[21] J. Noga, R.J. Bartlett, The full CCSDT model for molecular electronic structure, J. Chern. Phys. 86 (1987) 7041–7050.
[22] J. Noga, R.J. Bartlett, Erratum: The full CCSDT model for molecular electronic structure (J. Chem. Phys. 86 (1987) 7041-7050), J. Chem. Phys. 89 (1888) 3401.
[23] M.J. Frisch, et al., Gaussian 09, revision A.02; Gaussian, Inc., Wallingford, CT, 2009.
[24] A.I. Maergoiz, E.E. Nikitin, J. Troe, V.G. Ushakov, Classical trajectory and statistical adiabatic channel study of the dynamics of capture and unimolecular bond fission. IV. Valence interactions between atoms and linear rotors, J. Chem. Phys. 108 (1998) 5265–5280.
[25] A.I. Maergoiz, E.E. Nikitin, J. Troe, V.G. Ushakov, Classical trajectory and statistical adiabatic channel study of the dynamics of capture and unimolecular bond fission. V. Valence interactions between two linear rotors, J. Chem. Phys. 108 (1998) 9987–9998.
[26] A.I. Maergoiz, E.E. Nikitin, J. Troe, V.G. Ushakov, Classical trajectory and statistical adiabatic channel study of the dynamics of capture and unimolecular bond fission. VI. Properties of transitional modes and specific rate constants k(E, J), J. Chem. Phys. 117 (2002) 4201–4213.
[27] S. Glasstone, K.J. Laidler, H. Eyring, The Theory of Rate Processes: The Kinetics of Chemical Reactions, Viscosity, Diffusion and Electrochemical Phenomena, McGraw-Hill Book Company Inc., New York, 1941.
[28] A. Karton, N. Sylvetsky, J.M.L. Martin, W4–17: a diverse and high-confidence dataset of atomization energies for benchmarking high-level electronic structure methods, J. Comp. Chem. 38 (2017) 2063–2075.
[29] L.A. Curtiss, P.C. Redfern, K. Raghavachari, Assessment of Gaussian-4 theory for energy barriers, Chem. Phys. Lett. 499 (2010) 168–172.
[30] M. Quack, J. Troe, Specific rate constants of unimolecular processes. II. Adiabatic channel model, Ber. Bunsenges. Phys. Chem. 78 (1974) 240–252.
[31] M. Quack, J. Troe, Unimolecular Processes V: Maximum free energy criterion for the high pressure limit of dissociation reactions, Ber. Bunsenges. Phys. Chem. 81 (1977) 329–337.
[32] J. Troe, Theory of thermal unimolecular reactions at high pressures, J. Chern. Phys. 75 (1981) 226–237.
[33] C.J. Cobos, J. Troe, Theory of thermal unimolecular reactions at high pressures. II. Analysis of experimental results, J. Chem. Phys. 83 (1985) 1010–1015.
[34] J. Troe, From quantum chemistry to dissociation kinetics: what we need to know, Mol. Phys. 112 (2014) 2374–2383.
[35] J. Troe, The colourful world of complex-forming bimolecular reactions, J. Chem. Soc. Faraday Trans. 90 (1994) 2303–2317.
[36] C.J. Cobos, Theoretical analysis of the rate constants for the interestellar reaction N + OH → NO + H, Int. J. Chem. Kinet. 27 (1995) 219–233.
[37] M.P. Badenes, E. Castellano, C.J. Cobos, A.E. Croce, M.E. Tucceri, Rate coefficient

for the reaction FCO + $FC(O)O_2 \rightarrow 2$ FC(O)O at 296 K, Chem. Phys. Lett. 303 (1999) 482–488.
[38] L.B. Harding, A.I. Maergoiz, J. Troe, V.G. Ushakov, Statistical rate theory for the HO + O $\rightleftarrows HO_2 \rightleftarrows$ H + O_2 reaction system: SACM/CT calculations between 0 and 500 K, J. Chem. Phys. 113 (2000) 11019–11034.
[39] M.P. Badenes, E. Castellano, C.J. Cobos, A.E. Croce, M.E. Tucceri, Kinetics of the reactions of $FC(O)O_2$ radicals with F atoms and F_2, Chem. Phys. 253 (2000) 205–217.
[40] J. Troe, Towards a quantitative analysis of association reactions in the atmosphere, Chem. Rev. 103 (2003) 4565–4576.
[41] Cristian Buendía-Atencio, Carlos J. Cobos, Theoretical study of the thermochemistry and the kinetics of the SFxCl (x = 0–5) series, J. Fluor. Chem. 132 (2011) 474-481.
[42] Adela E. Croce, Carlos J. Cobos, Theoretical kinetics study of the reactions forming the ClCO radical cycle in the middle atmosphere of Venus, Z. Phys. Chem. 229 (2015) 1541–1559.
[43] W. Forst, Unimolecular rate theory test in thermal reactions, J. Phys. Chem. 76 (1972) 342–348.
[44] G.Z. Whitten, B.S. Rabinovitch, Accurate and facile approximation for vibrational energy-level sums, J. Chem. Phys. 38 (1963) 2466–2473.
[45] J. Troe, Theory of thermal unimolecular reactions at low pressures. II. Strong collision rate constants, Appl. J. Chem. Phys. 66 (1977) 4758–4775.
[46] J. Troe, Theory of thermal unimolecular reactions at low pressures I. Solutions of the master equation, J. Chem. Phys. 66 (1977) 4745–4757.
[47] H. Hippler, J. Troe, H.J. Wendelken, Collisional deactivation of vibrationally highly excited polyatomic molecules. II. Direct observation for excited toluene, J. Chem. Phys. 78 (1983) 6709–6717.
[48] H. Hippler, J. Troe, H.J. Wendelken, Collisional deactivation of vibrationally highly excited polyatomic molecules. III. Direct observation for substituted cycloheptatrienes, J. Chem. Phys. 78 (1983) 6718–6724.
[49] M. Heymann, H. Hippler, J. Troe, Collisional deactivation of vibrationally highly excited polyatomic molecules. IV. Temperature dependence of $< \Delta E >$, J. Chem. Phys. 80 (1984) 1853–1860.
[50] H. Hippler, L. Lindemann, J. Troe, Collisional energy transfer of vibrationally highly excited molecules. V. UV absorption study of azulene, J. Chem. Phys. 83 (1985) 3906–3912.
[51] H. Hippler, B. Otto, J. Troe, Collisional energy transfer of vibrationally highly excited molecules. VI. Energy dependence of $< \Delta E >$ in azulene, Ber. Bunsenges. Phys. Chem. 93 (1989) 428–434.
[52] J. Troe, V.G. Ushakov, Representation of broad fall-off curves for dissociation and recombination reactions, Z. Phys. Chem. 228 (2013) 1–10.
[53] J. Troe, Theory of thermal unimolecular reactions in the fall-off range. I. Strong collision rate constants, Ber. Bunsenges. Phys. Chem. 87 (1983) 161–169.
[54] J. Troe, Predictive possibilities of unimolecular rate theory, J. Phys. Chem. 83 (1979) 114–126.